

# Exceptional Mn<sup>II</sup> stability and Mn<sup>II</sup>/Zn<sup>II</sup> selectivity with rigid polydentate ligands

*Patrick Cieslik,<sup>a)†</sup> Peter Comba,<sup>a),b)\*</sup> Benedikt Dittmar,<sup>a)</sup>*

*Daouda Ndiaye,<sup>c)†</sup> Éva Tóth,<sup>c)\*</sup> Gunasekaran Velmurugan<sup>a)</sup> and Hubert Wadepohl<sup>a)</sup>*

a) Universität Heidelberg, Anorganisch-Chemisches Institut, INF 270, D-69120 Heidelberg, Germany

b) Universität Heidelberg, Interdisciplinary Center for Scientific Computing, INF 205, D-69120 Heidelberg, Germany

c) Centre de Biophysique Moléculaire, CNRS UPR 4301, Université d'Orléans, rue Charles Sadron, 45071 Orléans, France

† This work is part of the PhD theses of Patrick Cieslik and Daouda Ndiaye

Correspondence:

E-mail: peter.comba@aci.uni-heidelberg.de

eva.jakabtoth@cnrs.fr

## Abstract

While Mn<sup>II</sup> complexes meet increasing interest in biomedical applications, ligands are lacking that enable high stability and selectivity vs. Zn<sup>II</sup>, the most relevant biological competitor. We report here two new bispidine derivatives, which provide rigid and large coordination cavities that perfectly match the larger size of Mn<sup>II</sup> and yield eight-coordinate Mn<sup>II</sup> complexes with record stabilities. In contrast, the smaller Zn<sup>II</sup> ion cannot accommodate all ligand donors, resulting in highly strained and therefore less stable six-coordinate complexes. Combined theoretical and experimental data (X-ray crystallography, potentiometry, relaxometry and <sup>1</sup>H NMR spectroscopy) demonstrate unprecedented selectivity for Mn<sup>II</sup> vs. Zn<sup>II</sup> ( $K_{MnL}/K_{ZnL}$  of  $10^8$ - $10^{10}$ ), in sharp contrast to the usual Irving-Williams behavior, and record Mn<sup>II</sup> complex stabilities and inertness with  $\log K_{MnL}$  close to 25.

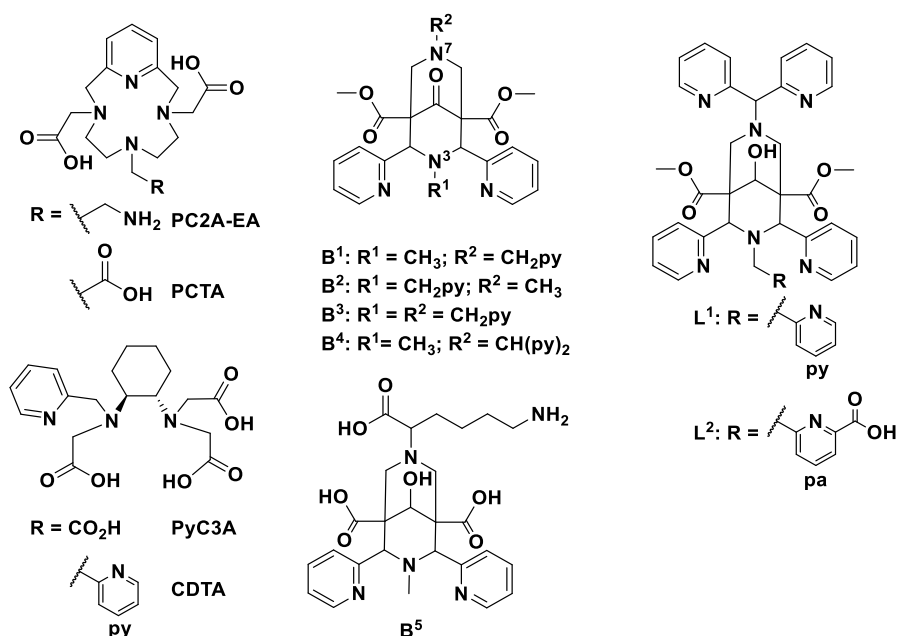
## Introduction

Manganese is an essential element for life. In biological systems, it can have a structural role or be involved in hydrolytic or redox transformations. Prominent examples are the oxidation of water to dioxygen in the oxygen evolving complex (OEC) in photosynthesis, the final reaction of the urea cycle catalyzed by arginase and the disproportionation of superoxide in the manganese-based superoxide dismutase (SOD).<sup>[1-5]</sup> Manganese complexes are also increasingly important in medicinal applications, *e.g.*, as SOD mimetics,<sup>[6-12]</sup> MRI contrast agents,<sup>[13,14]</sup> in chelation therapy of manganese overload and in-cell fluorescence tracking of the labile manganese pool.<sup>[15]</sup> Essential for most of these applications are high kinetic inertness, high complex stability and selectivity with respect to other ubiquitous first row transition metal cations, specifically Zn<sup>II</sup>, the most relevant and abundant biological competitor. From this follows the major challenge for Mn<sup>II</sup> devices and drugs, contrast agents and chelation therapy: due to the relatively large ionic radius of Mn<sup>II</sup> and the spherical distribution of the *d* electrons, Mn<sup>II</sup> complexes are intrinsically labile and the stability of Mn<sup>II</sup> coordination compounds with any particular ligand is generally one of the lowest among the first-row transition metal di-cations, and therefore lower than for the main biological competitor Zn<sup>II</sup>. The Irving-Williams series, established more than 70 years ago, describes the complex stability order of first row transition metal di-cations with a given ligand as Mn<sup>II</sup> < Fe<sup>II</sup> < Co<sup>II</sup> < Ni<sup>II</sup> < Cu<sup>II</sup> > Zn<sup>II</sup>,<sup>[16, 17]</sup> and this explains the lack of Mn<sup>II</sup> selective ligands. In biological systems, peculiar mechanisms help to exclude competitive metal ions from metalloprotein binding sites in need of weakly binding metal centers. For instance, local Mn<sup>II</sup> concentrations may be elevated in organelles such as the chloroplast or mitochondria or may increase in response to a stimulus (presence of an oxidant) to allow for the metalation in manganese-based SOD. In other cases, dedicated metal delivery systems or kinetic effects govern selectivity.<sup>[18, 19]</sup>

Three apparent design principles to achieve Mn<sup>II</sup> vs. Zn<sup>II</sup> selectivity are: (i) ligands that fully encapsulate the metal ion lead to slow metal ion exchange, (ii) a preference for Mn<sup>II</sup> over the other first row transition metal di-cations requires a large and rigid cavity – depending on the coordination number, the size of Mn<sup>II</sup> is approx. 10% larger than that of Zn<sup>II</sup>,<sup>[20]</sup> and (iii) a relatively large cavity imposed by a high denticity of an open-chained ligand may enforce one

of the pendant donor groups to be uncoordinated with a smaller competitor, leading to a decrease in bonding energy.

The bispidine scaffold ( $B^1$  -  $B^5$ ,  $L^1$ ,  $L^2$  in Scheme 1) is an ideal system to test these principles. It has the advantages of an established modular assembly and a large range of available ligands with a variety of denticities and donor group combinations.<sup>[21-27]</sup> Due to the rigidity of the tetradentate adamantane-derived platform and additional highly preorganized pendent donor groups, bispidine ligands are known to offer efficient complexation pathways and to form very inert complexes.<sup>[25]</sup> This has been shown in a number of studies with bispidine-based radioactive probes<sup>[25]</sup> and was also confirmed in a recent  $Mn^{II}$  based magnetic resonance imaging study with a pentadentate bispidine.<sup>[28]</sup> Importantly, the exceedingly rigid bispidine cavity is known to favor large metal ions,<sup>[25,29-31]</sup> and with penta- and hexadentate bispidines stability constants of first row transition metal di-cations have been observed that do not strictly follow Irving-Williams behavior.<sup>[21]</sup> Based on earlier observations with branched dipyridylamine donor groups,<sup>[31, 32]</sup> we therefore have designed and prepared the new hepta- and octadentate bispidines  $L^1$  and  $L^2$  that should efficiently encapsulate  $Mn^{II}$  and have at least one dangling donor function in the corresponding  $Zn^{II}$  complex, and therefore yield high selectivity for  $Mn^{II}$  in the presence of excess  $Zn^{II}$ .



**Scheme 1.** Ligands discussed in this manuscript.

With preparative and structural work, the evaluation of complex stabilities based on pH-potentiometry and relaxometric methods and combined with computational studies we show that bispidines L<sup>1</sup> and L<sup>2</sup> satisfy the prediction of unprecedented Mn<sup>II</sup> complex stability and selectivity over the main biological competitor Zn<sup>II</sup>.

## Syntheses, structural properties and molecular modeling

Ligands L<sup>1</sup> and L<sup>2</sup> were synthesized by slightly modifying previously reported procedures for the hexadentate ligand B<sup>4</sup>[<sup>31</sup>] The metal complexes were obtained from reaction of stoichiometric amounts of M(OTf)<sub>2</sub> (M = Mn<sup>II</sup>, Zn<sup>II</sup>) and ligand in acetonitrile (L<sup>1</sup>) or methanol (L<sup>2</sup>). Crystals, suitable for X-ray structure determination, were obtained by ether diffusion (see Supporting Information for details).

Plots of the solid state structures of [Mn(OTf)L<sup>1</sup>]OTf, [MnL<sup>2</sup>]OTf·0.2 H<sub>2</sub>O, [ZnL<sup>1</sup>](OTf)<sub>2</sub>·MeCN and [ZnL<sup>2</sup>]OTf are shown in Figure 1 and selected structural data are listed in Table 1 (also shown in Figure 1 are overlay plots of the two octa-coordinate Mn<sup>II</sup> structures and of the structures of the hexa-coordinate Zn<sup>II</sup> and the octa-coordinate Mn<sup>II</sup> complexes of L<sup>1</sup>). One of the Mn-N<sub>py</sub> bonds in both [Mn(OTf)L<sup>1</sup>]OTf (3.04 Å) and [MnL<sup>2</sup>]OTf·H<sub>2</sub>O (2.91 Å) are elongated but the corresponding pyridine nitrogen atoms have the lone pair oriented towards the metal center, *i.e.* there is an interaction between the Mn<sup>II</sup> center and the pyridine donor groups, shielding the former from coordination to further anions or solvent molecules.<sup>[24]</sup> Therefore, in both complexes, the Mn<sup>II</sup> ion is considered to be coordinated by all donors of the polydentate bispidine, and with L<sup>1</sup> a monodentate triflate anion completes the coordination sphere. That is, these Mn<sup>II</sup> complexes are rare examples of octa-coordinate Mn<sup>II</sup> ions,<sup>[33-37]</sup> and this supports the original hypothesis that the bispidine cavity is large and well suited for Mn<sup>II</sup>, and this might help to overcome the Irving-Williams series based hurdle for Mn<sup>II</sup> selectivity. The similarity between the two Mn<sup>II</sup> complexes is emphasized by the overlay of their X-ray structures (Figure 1e), and the misfit of the heptadentate bispidine for Zn<sup>II</sup> is visualized with the comparison of the ZnL<sup>1</sup> and MnL<sup>1</sup> structures in Figure 1f: the overlay plot suggests that the cavity provided by the heptadentate ligand is as predicted complementary for Mn<sup>II</sup>, and the additional metal-ligand bond may lead to Mn<sup>II</sup> selectivity. From the overlay of the Mn<sup>II</sup> structures it emerges that both Mn<sup>II</sup> complexes are octa-coordinate with very similar structures. In aqueous solution MnL<sup>1</sup> is expected to have a coordinated water

molecule and therefore might be a valuable MRI contrast agent, while in the L<sup>2</sup> based complex the Mn<sup>II</sup> center is completely encapsulated and should be very tightly bound.

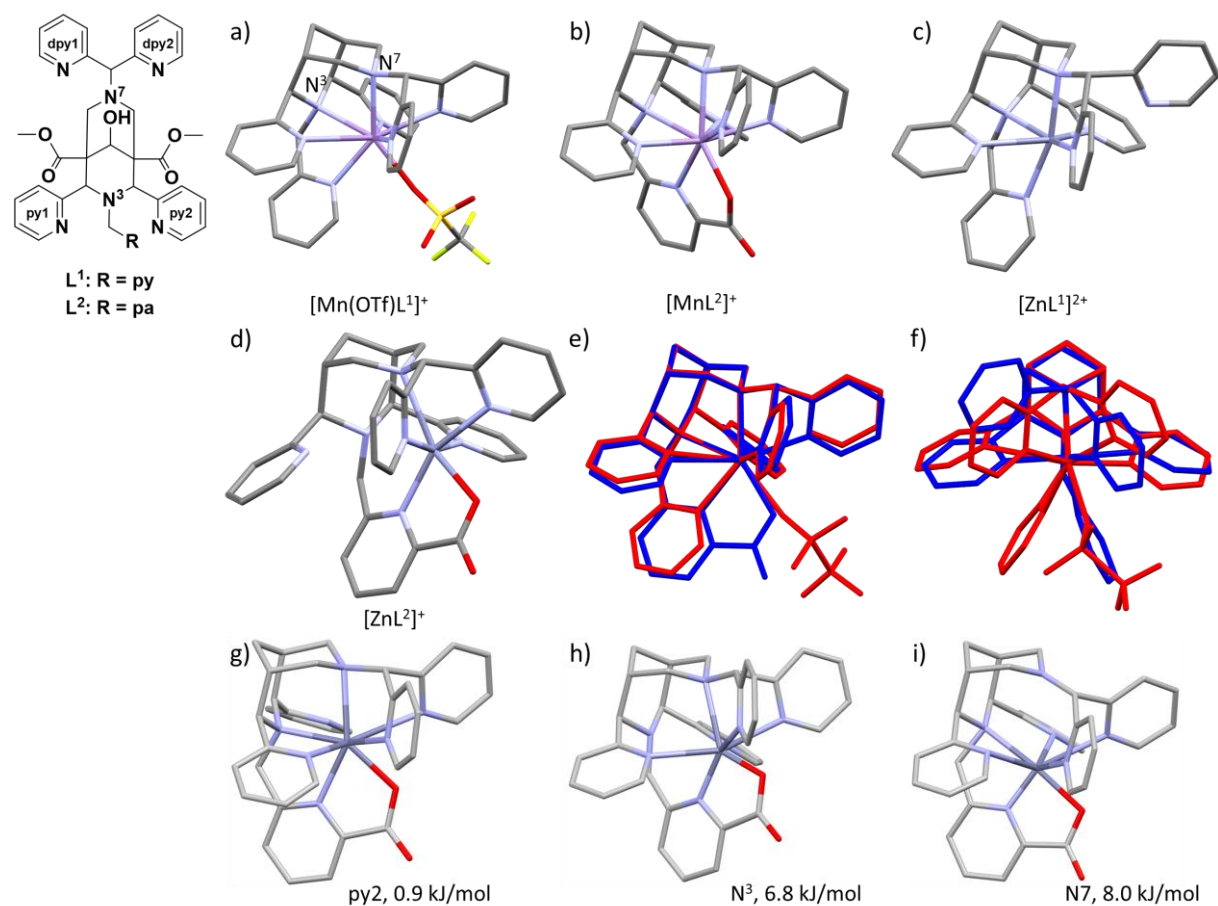


**Figure 1.** Experimental structures of the complex cations of a) [Mn(OTf)L<sup>1</sup>]OTf, b) [MnL<sup>2</sup>]OTf·0.2 H<sub>2</sub>O, c) [ZnL<sup>1</sup>](OTf)<sub>2</sub>·MeCN and d) [ZnL<sup>2</sup>]OTf, and X-ray structure overlay plots of e) [Mn(OTf)L<sup>1</sup>]<sup>+</sup> (red) and [MnL<sup>2</sup>]<sup>+</sup> (blue), and f) [Mn(OTf)L<sup>1</sup>]<sup>+</sup> (red) and [ZnL<sup>1</sup>]<sup>2+</sup> (blue), represented as capped sticks (hydrogen atoms, solvent molecules, anions, ester and hydroxy groups are omitted for clarity). ORTEP plots of the molecular cations of the X-ray analyses are given in the Supporting Information (Figure S3). g), h), i) are DFT optimized structures of [ZnL<sup>2</sup>]<sup>+</sup>; the donors given in the caption are those, which are elongated, and the energies are computed energies relative to the structure with an elongated Zn-py1 bond as in the crystal structure (computed metric parameters of all four optimized structures in comparison with the crystal structure are given in the Supporting Information, Table S4).

**Table 1.** Selected bond distances [Å] and angles [°] in the crystal structures of [Mn(OTf)L<sup>1</sup>]OTf, [MnL<sup>2</sup>]OTf·0.2 H<sub>2</sub>O, [ZnL<sup>1</sup>](OTf)<sub>2</sub>·MeCN and [ZnL<sup>2</sup>]OTf.

	[Mn(OTf)L <sup>1</sup> ]OTf	[MnL <sup>2</sup> ]OTf·0.2 H <sub>2</sub> O	[ZnL <sup>1</sup> ](OTf) <sub>2</sub> ·MeCN	[ZnL <sup>2</sup> ]OTf
Distance [Å]				
M-N3	2.4527(17)	2.3593(15)	2.155(3)	2.7449(11)
M-N7	2.4079(16)	2.5523(15)	2.208(3)	2.4791(11)
M-Npy1	3.037(2)	2.3635(18)	2.134(3)	3.8058(14)
M-Npy2	2.2937(19)	2.9098(22)	2.534(3)	2.1601(12)
M-D(N3)	2.2728(18)	2.2412(17)	2.149(3)	2.1363(12)
M-Ndpy1	2.2520(18)	2.4233(17)	3.374(4)	2.1643(12)
M-Ndpy2	2.5487(17)	2.3775(18)	2.059(3)	2.2300(12)
M-O <sub>x</sub>	2.3804(16)	2.2018(14)	-	2.1244(10)
Angle [°]				
N3-M-N7	72.42(5)	73.37(5)	83.26(11)	65.69(3)
Npy1-Mn-Npy2	130.92(6)	129.37(5)	149.46(11)	120.67(4)

In order to further demonstrate the perfect match of the two new bispidine ligands for Mn<sup>II</sup> and the misfit for Zn<sup>II</sup>, cavity shape and size calculations were performed with an established method based on empirical force field calculations,<sup>[38-40]</sup> where the steric strain enforced onto the ligand by coordination to a metal ion is plotted as a function of the metal ion size: the steric energy of the ligand is computed, while systematically changing the distances of the metal ion to all donor atoms under the conditions that (i) not all metal-donor distances change by the same amount (*i.e.* there are stronger and weaker bonds and asymmetric changes are tolerated), and (ii) the energies of the metal ligand bonds are not included in the computed total strain energy, *i.e.* these plots are metal-ion-independent. Importantly, this method allows asymmetric shapes of ligand cavities and the change of the ligand shape to be computed, and also to separate ligand-based strain from the energetics of metal-ligand interactions. Therefore, this technique is ideal to compare various metal ions with respect to their fit to a specific ligand, and this has been done successfully, specifically also with bispidine ligands, see Supporting Information for details.<sup>[24,25,29-31,50,51]</sup> From the plots in Figure 2a, where the metal ion induced ligand strain to L<sup>1</sup> and L<sup>2</sup> are shown for octa-coordination as observed for Mn<sup>II</sup>, it emerges that Mn<sup>II</sup> has the optimum size and Zn<sup>II</sup> is much too small and therefore induces ligand-based strain of approx. 50 kJ/mol. The vertical lines for Zn<sup>II</sup> and Mn<sup>II</sup> correspond to the average bond distances in the observed ML<sup>1</sup> and ML<sup>2</sup> structures (see Supporting Information for details). From the plot of the L<sup>1</sup> based complex using the hexacoordinate Zn<sup>II</sup> geometry with one dangling pyridine group (see Figure 1c for the

corresponding structure), the minimum of the curve is as expected shifted towards shorter bond lengths ( $d_{\min} = 2.15 \text{ \AA}$ , Figure 2b), which results in a better matching cavity for the smaller  $\text{Zn}^{\text{II}}$  ion while acting as a six-coordinate ligand.

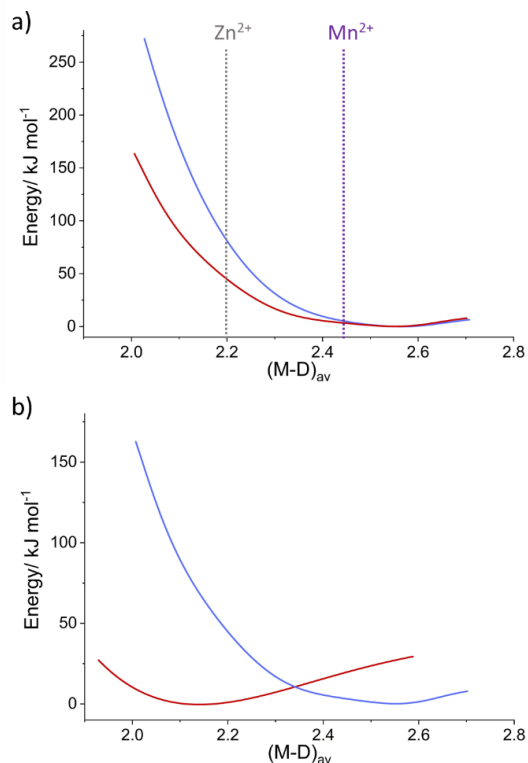


**Figure 2.** Hole-size curves (computed strain energy as a function of the averaged metal-donor bond distance  $(\text{M-D})_{\text{av}}$  (sum of all M-D distances divided by the number of the M-D bonds), all energy minima set to 0.0 kJ/mol) for a)  $\text{L}^1$  (red) and  $\text{L}^2$  (blue) with full coordination of all donors (octa-coordinate  $\text{Mn}^{\text{II}}$  and  $\text{Zn}^{\text{II}}$ ), and b) comparison of hole size curves of  $\text{L}^1$  with hexa-coordination (red, as observed for  $\text{Zn}^{\text{II}}$ ) and hepta-coordination (blue, as observed for  $\text{Mn}^{\text{II}}$ , where the  $\text{OH}_2$  co-ligand was omitted). Note that these energies do not include metal-ligand bonding.

The nature and relative energy of the interactions between the metal center and the ligands have also been evaluated by an energy decomposition analysis (EDA; B3LYP-D3/TZ2P with ZORA, see Supporting Information) to further analyze the putative selectivity of  $\text{L}^1$  and  $\text{L}^2$  for  $\text{Mn}^{\text{II}}$ .<sup>[41-43]</sup> The coordinates of the crystal structures of the four complexes (see Table 1) were optimized by DFT (density functional theory, using the Gaussian 16 suite of programs,<sup>[44]</sup> with the B3LYP-D3 functional, the LACVP basis set comprising the LanL2DZ-Los Alamos effective core potential for Mn<sup>[45-47]</sup> and a 6-31g(d) basis set<sup>[48]</sup> for the other atoms,<sup>[49]</sup> see Supporting Information for details). It appears that the metal-ligand interaction (also involving the coordinated triflate anion for the  $\text{MnL}^1$  complex) is more covalent in nature for the  $\text{Mn}^{\text{II}}$  than the  $\text{Zn}^{\text{II}}$  complex, and this might contribute to a larger bonding energy of the  $\text{Mn}^{\text{II}}$  complexes,



but the major part of the stabilization of  $Mn^{II}$  is due to the number of M-L bonds (octa- vs. hexa-coordination; see Supporting Information, Table S2). The computed bonding energy differences between the  $Mn^{II}$  and  $Zn^{II}$  complexes with  $L^1$  and  $L^2$  in favor for  $Mn^{II}$  translate to approx.  $\Delta(\log K)$  values of around 10 and 15, respectively (see Supporting Information). Taking into consideration the approximations used and the intrinsic problems of DFT to describe metal ligand bonds, these predictions are well supporting the observed stability constants discussed below, *i.e.* the  $Mn^{II}$  selectivity is of the order of 10 orders of magnitude, with  $L^2$  being more selective than  $L^1$ .

A closer look at the crystal structures of the  $ZnL^1$  and  $ZnL^2$  (see Figure 1) suggests that there are various positions for a small metal ion such as  $Zn^{II}$  in the rigid and too large bispidine cavity, *i.e.* there is a plateau in the potential energy surface with various shallow minima as observed in bispidine coordination chemistry before.<sup>[29, 50, 51]</sup> The result is a highly dynamic system with a series of different structures of similar energy (distortional isomers), and some of these have been optimized and are shown in Figure 1 (see also Supporting Information, Table S3). It follows that the observed crystal structures might not well enough describe the solution structures and dynamics of importance for the solution complex stabilities discussed below.

### Complex stabilities, $Mn^{II}/Zn^{II}$ selectivity and kinetic inertness

The complex stability constants were determined by potentiometry ( $MnL^1$ ,  $ZnL^1$ ,  $CaL^1$ ,  $ZnL^2$  and  $CaL^2$ ) or from the pH-dependent variation of longitudinal ( $MnL^1$ ) or transverse ( $MnL^2$ ) relaxation rates measured in aqueous solution containing equimolar quantities of  $Mn^{II}$  and the ligand. Although complexation of tetra-, penta- and hexadentate bispidines with divalent first row transition metal cations is typically very fast<sup>[25, 52]</sup> and  $Mn^{II}$  is known to be labile,  $Mn^{II}$  complex formation with  $L^1$  and  $L^2$  was unexpectedly slow, preventing direct titrations (complex formation could be also followed by UV-vis spectroscopy, see SI). Therefore,  $MnL^1$  and  $MnL^2$  stability constants were determined in batch samples with 6-75 hrs equilibration time depending on pH. Complex formation becomes faster when the pH increases, and this is expected due to base catalysis, as generally observed for poly(amino carboxylate) complexes.<sup>[53]</sup> Slow complexation was previously reported for  $MnB^5$ <sup>[28]</sup> as well as for  $Bi^{III}$  complexes of hepta- and octadentate bispidine ligands.<sup>[26]</sup> For the latter, an unstable complex

forms in a fast pre-equilibrium that requires heating to yield the final, stable product. With the  $MnL^1$  system, the formation of a pre-complex ( $MnL^{1*}$ ) and its protonated forms  $MnHL^{1*}$ ,  $MnH_2L^{1*}$  and  $MnH_3L^{1*}$  were observed above pH 4 by direct potentiometric titration, yielding stability constants with good reproducibility ( $\log K_{MnL^{1*}} = 8.45(5)$ ;  $\log K_{MnHL^{1*}} = 9.01(4)$ ;  $\log K_{MnH_2L^{1*}} = 5.98(3)$ ;  $\log K_{MnH_3L^{1*}} = 3.61(5)$ ). This pre-complex is 16 orders of magnitude less stable than the final product and likely corresponds to an „out-of-cage structure”, where the  $Mn^{II}$  ion has not yet entered the bispidine cavity. From the titration curves (Supporting Information, Figures S12, S13) it follows that a tertiary amine of the bispidine skeleton remains protonated in  $MnHL^{1*}$  in basic solution (deprotonation occurs with  $\log K_{HMnL^{1*}} = 9.01$ ).

In contrast to the  $Mn^{II}$  analogues,  $CaL^1$ ,  $CaL^2$ ,  $ZnL^1$  and  $ZnL^2$  form rapidly and the stability constants were determined from direct potentiometric titrations. The form of the titration curves demonstrates qualitatively but unambiguously the higher stability of  $MnL$  (*i.e.* the  $MnL$  titration curves run below those of the other systems), and that in the  $Zn^{II}$  and  $Ca^{II}$  complexes of both ligands, a tertiary amine remains protonated until basic pH (see Supporting Information, Figures S12, S13). This is supported by the DFT calculations that indicate energy minima structures with very weak and long  $Zn \cdots N(\text{amine})$  bonds (see above and Table S3).

For  $ZnL^2$ , the species distribution curves were corroborated by pH-dependent  $^1H$  NMR and UV-vis data recorded in aqueous solution. Changes in the  $^1H$  NMR spectra (in particular the chemical shift of the methylene protons of the bispidine skeleton, see Figure 3d) and in the UV-vis spectra (Supporting Information, Figure S15) correspond to pH regions where formation of the protonated (pH 1.0-3.0) or deprotonated complex (pH 7.4-10.0) occur. Complex formation can be directly monitored by the separation of the  $^1H$  NMR signals for the two methylene protons of the bispidine skeleton, resulting from a loss of flexibility of the bispidine due to metal binding (Supporting Information, Figure S14). Interestingly, the  $^1H$  NMR (Figure 3d) and UV-vis (Figure S15) changes corroborate an additional process at pH 4.5-6.5 which, according to the potentiometric titration, does not involve a deprotonation equilibrium, suggesting that this transformation corresponds to an internal rearrangement of the complex. This is supported by the structural observations and the DFT calculations that indicate a plateau with various isomeric shallow minima structures (see above, Figure 1).

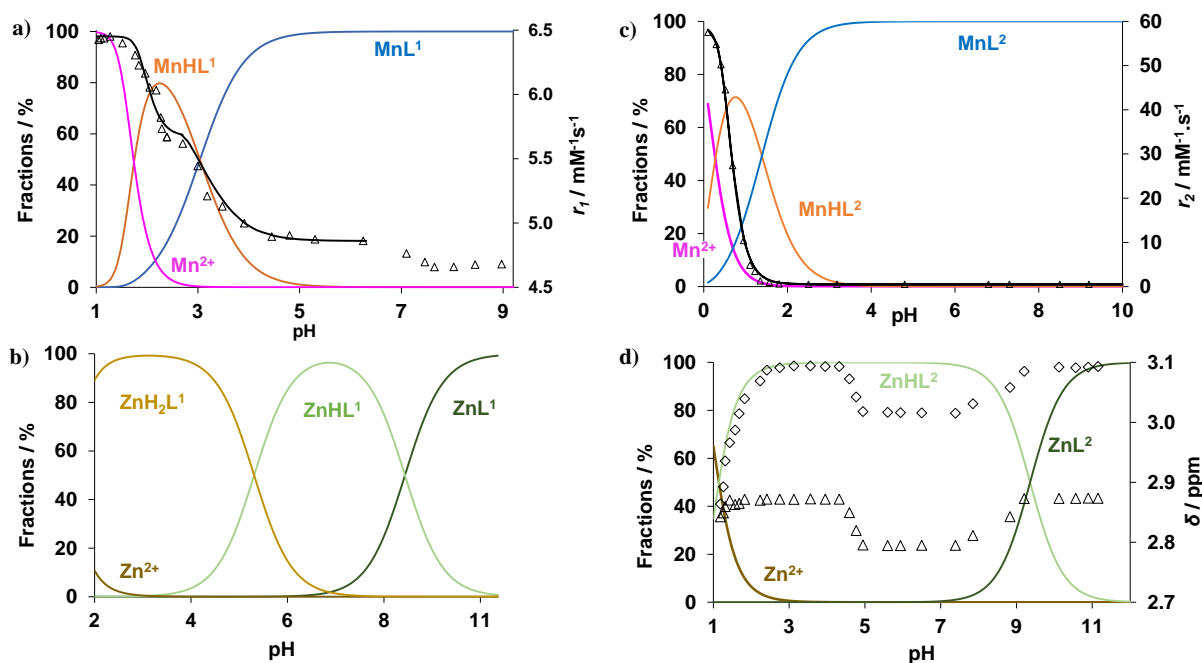


**Figure 3.** Species distribution curves calculated for MnL<sup>1</sup> a), ZnL<sup>1</sup> b), MnL<sup>2</sup> c) and ZnL<sup>2</sup> d) (1 mM concentration), pH-dependent relaxivities ( $\Delta$ ) measured at 25°C, 60 MHz for MnL<sup>1</sup> a) and MnL<sup>2</sup> b) (the black line represents the fit to yield stability constants), and pH-dependent chemical shifts of methylene protons ( $\diamond$  and  $\Delta$ ) of the bispidine skeleton for ZnL<sup>2</sup> d).

All fitted stability constants are collected in Table 2 and compared to  $\log K_{ML}$  values of representative literature examples (see Scheme 1 for ligand structures). For a more meaningful comparison of complex stabilities of ligands with different basicity, we have also calculated  $pM$  values ( $pM = -\log[M_{free}]$ ; at pH 7.4 and  $10^{-5}$  M total ligand and metal concentrations). Species distribution curves are shown in Figure 3. The first protonation constant  $\log K_{H1}$  for L<sup>1</sup>, needed for the calculation of the stability constants of MnL<sup>1</sup> and ZnL<sup>1</sup>, had to be estimated (see Supporting Information), leading to a possible systematic underestimation of the complex stabilities. However, this influences neither the ratio between the Mn<sup>II</sup> and Zn<sup>II</sup> complex stabilities, nor the  $pM$  values.

**Table 2.** Ligand protonation constants, Mn<sup>II</sup>, Zn<sup>II</sup> and Ca<sup>II</sup> stability constants and pM values for the hepta- and octadentate bispidines L<sup>1</sup> and L<sup>2</sup> and for reference ligands. Errors indicated in parenthesis correspond to one standard deviation. I = 0.15 M NaCl

	L <sup>1</sup>	L <sup>2</sup>	B <sup>5</sup> [28]	PyC3A [54]	trans-CDTA [55]	PC2A-EA [56]
logK <sub>H1</sub>	>11.05 <sup>a</sup>	11.9(2)	11.44	10.16	9.36	11.34
logK <sub>H2</sub>	6.73(5)	5.44(2)	10.31	6.39	5.95	8.93
logK <sub>H3</sub>	5.62(6)	5.28(2)	4.71	3.13	3.62	6.91
logK <sub>H4</sub>	5.27(6)	1.36(2)	2.76	-	2.57	1.97
logK <sub>H5</sub>	2.3(5)	-	2.22	-	-	-
logK <sub>MnL</sub>	24.20(4) <sup>b</sup> 24.4(2) <sup>c</sup>	24.7(2) <sup>c</sup>	12.21	14.14	14.32	19.01
logK <sub>MnHL</sub>	3.04(3) <sup>b</sup> 3.0(4) <sup>c</sup>	-	10.42	2.43	2.90	6.88
logK <sub>MnH2L</sub>	-	-	3.87	-	1.89	2.50
logK <sub>ZnL</sub>	15.11(5)	14.70(8)	15.59	-	16.75	-
logK <sub>ZnHL</sub>	9.18(3)	9.36(5)	10.33	-	2.57	-
logK <sub>ZnH2L</sub>	5.61(2)	-	3.28	-	-	-
logK <sub>CaL</sub>	8.76(3)	7.26(5)				
logK <sub>CaHL</sub>	11.05(2)	10.98(3)				
logK <sub>CaH2L</sub>	5.83(2)	3.84(6)				
logK <sub>CaH3L</sub>	4.39(8)	3.41(4)				
pMn <sup>d</sup>	12.73	12.59	6.65	8.17	8.68	9.27
pZn <sup>d</sup>	9.08	8.58	8.28			
pCa <sup>d</sup>	6.84	5.71				

[a]: lowest limit estimated from logK<sub>H1</sub> of CaL<sup>1</sup>; [b]: from potentiometry; [c]: from relaxometric titration; [d]: pM calculated for c<sub>M</sub> = c<sub>L</sub> = 10<sup>-5</sup> M, pH = 7.4.

The stability constants confirm the expectation from the ligand design and the structural and computational studies: the rigid and large bispidine scaffold and the pendant pyridine or picolinate donor groups perfectly wrap around the Mn<sup>II</sup> ion, leading to record stabilities for MnL<sup>1</sup> and MnL<sup>2</sup>. The pMn values, particularly relevant for biological applications of Mn<sup>II</sup> complexes, with 12.73 and 12.59 for MnL<sup>1</sup> and MnL<sup>2</sup>, respectively, are substantially higher than those of complexes considered particularly stable, such as MnDOTA (pMn = 9.02),<sup>[57]</sup> MnPC2A-EA (pMn = 9.27),<sup>[56]</sup> or MnPCTA with the highest published value for an Mn<sup>II</sup> complex (pMn = 9.74).<sup>[58]</sup> Most importantly, with the bispidines L<sup>1</sup> and L<sup>2</sup> we observe unprecedented selectivity for Mn<sup>II</sup> vs. Zn<sup>II</sup>, amounting to 9.1 and 10.0 logK units, respectively (differences in the pM values of 3.65 and 4.01, respectively): these ligands represent the first examples of real and efficient Mn<sup>II</sup> selectivity in aqueous solution. Indeed, the IUPAC Stability Constants Database (<http://www.acadsoft.co.uk/>) contains only few examples of Mn<sup>II</sup>/Zn<sup>II</sup> selectivity with logK differences below 1, not comparable with our results.

The stability constant of  $\text{CuL}^1$  is too high to be calculated from the potentiometric titration curve (see Supporting Information), as the complex is fully formed at pH 1.8. We have estimated the lower limit as  $\log K_{\text{CuL}^1} > 26$ , indicating that the  $\text{Mn}^{2+}$  selectivity of  $\text{L}^1$  (and  $\text{L}^2$ ) is not retained for  $\text{Cu}^{2+}$ . This is an interesting and as yet not fully understood observation. However, experience indicates that  $\text{Cu}^{\text{II}}$  has a well-fitting shape for the bispidine cavity, and the known  $\text{Cu}^{\text{II}}$ -bispidine complexes generally have very high complex stabilities.<sup>[25],29, 50, 51]</sup> A thorough analysis of the  $\text{Cu}^{\text{II}}$  stabilities with  $\text{L}^1$  and  $\text{L}^2$  will require knowledge on the solution structural properties of these complexes, and this is missing at the moment.

Finally, we have also assessed the kinetic inertness of  $\text{MnL}^1$  in trans-metalation experiments with  $\text{Cu}^{2+}$ , in the pH range 2.3-3.5, by using an excess of  $\text{Cu}^{2+}$  to ensure pseudo-first order conditions and via monitoring the transverse proton relaxation rates (see SI). The observed rate constants are independent of pH which indicate that the proton-assisted dissociation pathway is negligible. A dissociation half-life of approx. 100 days has been estimated by extrapolating for physiological conditions, which places it among the most inert monohydrated  $\text{Mn}^{\text{II}}$  complexes known to date.<sup>[59]</sup>

## Conclusion

The new hepta- ( $\text{L}^1$ ) and octadentate bispidines ( $\text{L}^2$ ) form octa-coordinate  $\text{Mn}^{\text{II}}$  complexes with unprecedented stability ( $K_{\text{MnL}}$  values 5 orders of magnitude higher than for the best-known systems) and  $\text{Mn}^{\text{II}}/\text{Zn}^{\text{II}}$  selectivity (8-10 orders of magnitude higher  $\text{Mn}^{\text{II}}$  than  $\text{Zn}^{\text{II}}$  stabilities). Beating the Irving-Williams series is difficult and rare. With the ligands presented here, this success is based on the large and rigid diazaadamantane-derived cavity of the bispidine scaffold that is ideally suited for  $\text{Mn}^{\text{II}}$ , allowing for eight-coordination. In contrast, competitors such as  $\text{Zn}^{\text{II}}$  are too small for the cavity and allow only 6 of the 7 or 8 potential donors to efficiently bind to the metal center, leading both to a lower binding energy and to increased ligand-based steric strain. While the octadentate ligand  $\text{L}^2$  fully encapsulates  $\text{Mn}^{\text{II}}$  and provides the highest  $\text{Mn}^{\text{II}}$  complex stability known so far, the  $\text{Mn}^{\text{II}}$  complex of the heptadentate ligand  $\text{L}^1$  has one inner-sphere water in aqueous solution. Therefore,  $\text{MnL}^1$  may be of interest as an MRI contrast agent. Indeed, it has a remarkably good relaxation efficiency, with a longitudinal proton relaxivity of  $5.04 \text{ mM}^{-1}\text{s}^{-1}$  at 20 MHz, 25°C (see SI for full Nuclear Magnetic Relaxation Dispersion profiles), 20 % higher than that of the clinically used contrast

agent GdDOTA ( $4.2 \text{ mM}^{-1}\text{s}^{-1}$  under the same conditions). Complexes of both  $L^1$  and  $L^2$  and of further derivatives may find applications in applications, where large complex stabilities and slow metal exchange rates are of importance, *e.g.* Positron Emission Tomography (PET) with  $^{52}\text{Mn}$ .

## Supporting Information

The Supporting Information includes all experimental details, the crystallographic data and information on the structural refinement, computational details, NMR spectra as well as the data on potentiometry and relaxivity measurements of the ligands and complexes.

## Acknowledgements

Financial support by Heidelberg University, the German Science Foundation (Deutsche Forschungsgemeinschaft, DFG) and ANR (Agence Nationale de la Recherche, France) is gratefully acknowledged. This study was conducted within the Max Planck School Matter to Life, supported by the German Federal Ministry of Education and Research (BMBF) in collaboration with the Max Planck Society. We are grateful for computational resources provided by the bwForCluster JUSTUS, funded by the Ministry of Science, Research and Arts and the Universities of the State of Baden-Württemberg, Germany, within the framework program bwHPC-C5.

## Conflicts of interest

The authors declare no conflicts of interest.

## References

- [1] R. J. P. Williams, in *Bioinorganic Chemistry* (Eds.: H. B. Kraatz, N. Metzler-Nolte), Wiley, Weinheim, **2006**.
- [2] D. Christianson, *Prog. Biophys. Mol. Biol* **1997**, *67*, 217-243.
- [3] N. A. Law, M. T. Caudle, V. L. Pecoraro, *Adv. Inorg. Chem.* **1998**, *46*, 305-440.
- [4] K. M. Erikson, M. Ascher, in *Metal ions in life sciences, Vol. 19* (Eds.: A. Sigel, E. Freisinger, R. K. O. Sigel), **2019**, pp. 253-266.
- [5] D. P. Riley, *Chem. Rev.* **1999**, *99*, 2573-2587.
- [6] D. P. Riley, R. H. Weiss, *J. Am. Chem. Soc.* **1994**, *116*, 387-388.

- [7] K. Barnese, E. B. Gralla, J. S. Valentine, D. E. Cabelli, *Proc. Natl. Acad. Sci. USA* **2012**, *109*, 6892-6897.
- [8] D. Salvemini, D. P. Riley, S. Cuzzocrea, *Nature Rev. Drug Discovery* **2002**, *1*, 367-374.
- [9] C. X. Zhang, S. J. Lippard, *Curr. Opin. Chem. Biol.* **2003**, *7*, 481-489.
- [10] P. Chen, S. Chakraborty, S. Mukhopadhyay, E. Lee, M. M. B. Paoliello, A. B. Bowman, M. Aschner, *J. Neurochem.* **2015**, *134*, 601-610.
- [11] I. Ivanovic-Burmazovic, M. R. Filipovic, *Adv. Inorg. Chem.* **2012**, *64*, 53-95.
- [12] L. Senft, J. L. Moore, A. Franke, K. R. Fisher, A. Scheitler, A. Zahl, R. Puchta, D. Fehn, S. Ison, S. Sader, I. Ivanovic-Burmazovic, C. R. Goldsmith, *Chem. Sci.* **2021**, *12*, 10483-10500.
- [13] B. Drahos, I. Lukes, E. Toth, *Eur. J. Inorg. Chem.* **2012**, *12*, 1975-1986.
- [14] A. Gupta, P. Caravan, W. S. Price, C. Platas-Iglesias, E. M. Gale, *Inorg. Chem.* **2020**, *59*, 6648-6678.
- [15] S. Bakthavatsalam, A. Sarkar, A. Rakshit, S. Jin, A. Kumar, A. Datta, *Chem. Commun.* **2015**, *51*, 2605-2608.
- [16] H. Irving, R. J. P. Williams, *Nature* **1948**, *162*, 746-747.
- [17] D. A. Johnson, P. G. Nelson, *Inorg. Chem.* **1995**, *34*, 5655-5671.
- [18] A. W. Foster, D. Osman, N. J. Robinson, *J. Biol. Chem.* **2014**, *289* (41), 28095-28103.
- [19] K. M. Erikson, M. Aschner, *Met Ions Life Sci.* **2019**, *14*, 19.
- [20] R. Shannon, *Acta. Crystallogr., Sect. A32* **1976**, *32*, 751-767.
- [21] K. Born, P. Comba, R. Ferrari, G. A. Lawrance, H. Wadepohl, *Inorg. Chem.* **2007**, *46*, 458-464.
- [22] A. M. Nonat, A. Roux, M. Sy, L. J. Charbonniere, *Dalton Trans.* **2019**, *48*, 16476-16492.
- [23] P. Comba, B. Nuber, A. Ramlow, *J. Chem. Soc., Dalton Trans.* **1997**, 347-352.
- [24] P. Comba, U. Jermilova, C. Orvig, B. O. Patrick, C. F. Ramogida, K. Rück, C. Schneider, M. Starke, *Chem. Eur. J.* **2017**, *23*, 15945-15956.
- [25] P. Comba, M. Kerscher, K. Rück, M. Starke, *Dalton Trans.* **2018**, *47*, 9202-9220.
- [26] F. Bruchertseifer, P. Comba, B. Martin, A. Morgenstern, J. Notni, M. Starke, H. Wadepohl, *ChemMedChem.* **2020**, *15*, 1591-1600.
- [27] L. Abad-Galan, P. Cieslik, P. Comba, M. Gast, O. Maury, L. Neupert, A. Roux-Gossart, H. Wadepohl, *Chem. Eur. J.* **2021**, *27*, 10303-10312.
- [28] D. Ndiaye, M. Sy, A. Pallier, S. Meme, I. d. Silva, S. Lacerda, A. M. Nonat, L. J. Charbonniere, E. Toth, *Angew. Chem. Int. Ed. Engl.* **2020**, 11958-11963.
- [29] P. Comba, M. Kerscher, M. Merz, V. Müller, H. Pritzkow, R. Remenyi, W. Schiek, Y. Xiong, *Chem. Eur. J.* **2002**, *8*, 5750-5760.
- [30] C. Bleiholder, H. Börzel, P. Comba, R. Ferrari, A. Heydt, M. Kerscher, S. Kuwata, G. Laurency, G. A. Lawrance, A. Lienke, B. Martin, M. Merz, B. Nuber, H. Pritzkow, *Inorg. Chem.* **2005**, *44*, 8145-8155.
- [31] P. Comba, H. Rudolf, H. Wadepohl, *Dalton Trans.* **2015**, *44* (6), 2724-2736.
- [32] P. V. Bernhardt, P. Comba, A. Mahu-Rickenbach, S. Stebler, S. Steiner, K. Várnagy, M. Zehnder, *Inorg. Chem.* **1992**, *31*, 4194.
- [33] K. Neupert-Laves, M. Dobler, *Helv. Chim. Acta* **1977**, *60*, 1861-1871.
- [34] H. O. Reid, I. A. Kahwa, A. J. White, D. J. Williams, *Inorg. Chem.* **1998**, *37*, 3868-3873.
- [35] D. B. Dang, Y. Bai, C. Y. Duan, *J. Chem. Crystallogr.* **2008**, *38*, 557-560.
- [36] S. Wang, T. D. Westmoreland, *Inorg. Chem.* **2009**, *48*, 719-727.
- [37] K. S. Dube, T. C. Harrop, *Dalton Trans.* **2011**, *40*, 7496-7498.
- [38] P. Comba, N. Okon, R. Remenyi, *J. Comput. Chem.* **1999**, *20*, 781-785.

- [39] P. Comba, T. W. Hambley, G. Lauer, N. Okon, *MOME97, a molecular modeling package for inorganic compounds*, Heidelberg, **1997**.
- [40] P. Comba, T. W. Hambley, M. Ströhle, *Helv. Chim. Acta.* **1995**, *78*, 2042-2047.
- [41] K. Morokuma, *J. Chem. Phys.* **1971**, *55*, 1236-1244.
- [42] T. Ziegler, A. Rauk, *Theor. Chim. Acta* **1977**, *46*, 1.
- [43] G. te Velde, F. M. Bickelhaupt, E. J. Baerends, C. Fonseca Guerra, S. J. A. van Gisbergen, J. G. Snijders, T. Ziegler, *J. Comp. Chem.* **2001**, *22*, 931-967.
- [44] M. J. Frisch, G. W. Trucks, H. B. Schlegel, G. E. Scuseria, M. A. Robb, J. R. Cheeseman, G. Scalmani, V. Barone, G. A. Petersson, H. Nakatsuji, X. Li, M. Caricato, A. V. Marenich, J. Bloino, B. G. Janesko, R. Gomperts, B. Mennucci, H. P. Hratchian, J. V. Ortiz, A. F. Izmaylov, J. L. Sonnenberg, D. Williams-Young, F. Ding, F. Lipparini, F. Egidi, J. Goings, B. Peng, A. Petrone, T. Henderson, D. Ranasinghe, V. G. Zakrzewski, J. Gao, N. Rega, G. Zheng, W. Liang, M. Hada, M. Ehara, K. Toyota, R. Fukuda, J. Hasegawa, M. Ishida, T. Nakajima, Y. Honda, O. Kitao, H. Nakai, T. Vreven, K. Throssell, J. A. Montgomery Jr., J. E. Peralta, F. Ogliaro, M. J. Bearpark, J. J. Heyd, E. N. Brothers, K. N. Kudin, V. N. Staroverov, T. A. Keith, R. Kobayashi, J. Normand, K. Raghavachari, A. P. Rendell, J. C. Burant, S. S. Iyengar, J. Tomasi, M. Cossi, J. M. Millam, M. Klene, C. Adamo, R. Cammi, J. W. Ochterski, R. L. Martin, K. Morokuma, O. Farkas, J. B. Foresman, D. J. Fox, Wallingford, CT, **2016**.
- [45] P. J. Hay, W. R. Wadt, *J. Chem. Phys.* **1985**, *82*, 270-283.
- [46] W. R. Wadt, P. J. Hay, *J. Chem. Phys.* **1985**, *82*, 284-298.
- [47] P. J. Hay, W. R. Wadt, *J. Chem. Phys.* **1985**, *82*, 299-310.
- [48] R. Ditchfield, W. J. Hehre, J. A. Pople, *J. Chem. Phys.* **1971**, *54*, 724.
- [49] S. Grimme, J. Antony, S. Ehrlich, H. Krieg, *J. Chem. Phys.* **2010**, *132*, 154104.
- [50] P. Comba, W. Schiek, *Coord. Chem. Rev.* **2003**, *238-239*, 21-29.
- [51] K. Born, P. Comba, M. Kerscher, G. Linti, H. Pritzkow, H. Rohwer, *Dalton* **2009**, 362-367.
- [52] P. Comba, M. Kerscher, W. Schiek, *Prog. Inorg. Chem.* **2007**, *55*, 613-704.
- [53] E. Szilágyi, É. Tóth, Z. Kovács, J. Platzek, B. Radüchel, E. Brücher, *Inorg. Chim. Acta* **2000**, *298*, 226-234.
- [54] E. M. Gale, I. P. Atanasova, F. Blasi, I. Ay, P. Caravan, *J. Am. Chem. Soc.* **2015**, *137*, 15548-15557.
- [55] E. Molnár, B. Váradi, Z. Garda, R. Botár, F. K. Kálmán, É. Tóth, C. Platas-Iglesias, I. Tóth, E. Brücher, G. Tircsó, *Inorg. Chim. Acta* **2018**, *472*, 254-263.
- [56] R. Botár, E. Molnár, G. Trencsényi, J. Kiss, F. K. Kálmán, G. Tircsó **2020**, 1662-1666, *J. Am. Chem. Soc.* **2020**, *142*, 1662-1666.
- [57] A. Takacs, R. Napolitano, M. Purgel, A. C. Benyei, L. Zekany, E. Brucher, I. Toth, Z. Baranyai, S. Aime, *Inorg. Chem.* **2014**, *53*, 2858-2872.
- [58] Z. Garda, E. Molnár, F. K. Kálmán, R. Botár, V. Nagy, Z. Baranyai, E. Brücher, Z. Kovács, I. Tóth, G. Tircsó, *Front. Chem.* **2018**, *6*, 1-14.
- [59] S. Lacerda, D. Ndiaye, É. Tóth, in *Advances in Inorganic Chemistry, Vol. 78* (Eds.: C. D. Hubbard, E. v. Eldik), **2021**, pp. 109-142.